Nanoscale

RSC Publishing

PAPER

View Article Online
View Journal | View Issue

Cite this: *Nanoscale*, 2013, **5**, 9340

Al^{3+}-induced far-red fluorescence enhancement of conjugated polymer nanoparticles and its application in live cell imaging†

Heng Liu,‡[a] Xian Hao,‡[b] Chunhui Duan,‡[c] Hui Yang,‡[ad] Yi Lv,[a] Haijiao Xu,[b] Hongda Wang,*[b] Fei Huang,*[c] Debao Xiao[d] and Zhiyuan Tian*[a]

Fluorescent nanoparticles (NPs) for Al^{3+} sensing with high selectivity were developed from a type of carbazole-based conjugated polymer with a two-dimensional donor–π bridge–acceptor (D–π–A) structure. These NPs are characterized by their small particle diameter (~18 nm), far-red fluorescence emission (centered ~710 nm), and Al^{3+}-induced fluorescence enhancement with high selectivity owing to an Al^{3+}-triggered inhibition on the intramolecular charge transfer (ICT) processes between the conjugated backbone and the pendant acceptors. This type of nanoparticle is easily suspended in aqueous solutions, indicating their practical applicability in physiological media, and their ability for intracellular Al^{3+} sensing was confirmed. As compared to other types of conjugated polymer based probes showing metal ion mediated fluorescence quenching, these as-prepared NPs possess analyte-enhanced fluorescence emission, which is analytically favored in terms of sensitivity and selectivity. Fluorescence emission with wavelengths in the biological window of maximum optical transparency (~700 to 1000 nm) is expected to impart a salient advantage for biological detection applications to these as-prepared probes. The superior features of merit of this new type of fluorescent probe, together with the validation of practicability for intracellular Al^{3+} ion sensing, are indicative of their potential for application in fluorescence-based imaging and sensing, such as investigations on Al^{3+}-related physiological and pathological processes.

Received 16th May 2013
Accepted 12th July 2013

DOI: 10.1039/c3nr02522e

www.rsc.org/nanoscale

1 Introduction

Aluminum is the third most abundant element in the earth's crust and the general population is widely exposed to aluminum owing to its widespread use in daily life, such as in water treatment, food additives, aluminum-based pharmaceuticals, and storage/cooking utensils.[1] Aluminum can be found in living cells and biological fluids in its ionic form, Al^{3+}. It is well-known that aluminum is not an essential element for biological life and it exerts markedly adverse effects on human health.[2,3] Specifically, the superfluous ingestion of aluminum has been associated with osteoporosis and anemia by affecting the absorption of calcium in the bowel and iron in the blood, respectively.[4] More importantly, Al^{3+} has become prominent in the study of biochemistry centered on the toxicity of metal ions because it has been proposed to be a factor contributing to the etiology of a variety of neurological disorders in humans.[5] For instance, it has been demonstrated that aluminum exerts significant effects on the intracellular protein turnover and consequently leads to an imbalance of photolytic and anti-proteolytic systems in cellular life,[6] which is supposed to be a crucial factor responsible for the onset of Alzheimer's[7] and Parkinson's diseases,[8] and intoxication in hemodialysis patients.[5] These adverse health effects make Al^{3+} an important target in metal ion recognition and it is therefore crucial to develop sensors for the facile detection of Al^{3+} with high sensitivity and selectivity in biological systems.

Fluorescent probes for the real-time sensing of biologically important ions and *in vivo* fluorescence imaging have become indispensable tools in the fields of bioimaging, clinical diagnosis, modern medicine, and biological sciences. However, as compared to other metal ions, the detection of Al^{3+} has been problematic owing to the lack of spectroscopic characteristics and poor coordination ability of Al^{3+}.[9] To date, only limited

[a]*School of Chemistry and Chemical Engineering, University of Chinese Academy of Sciences (UCAS), Beijing 100049, China. E-mail: zytian@ucas.ac.cn*

[b]*State Key Laboratory of Electroanalytical Chemistry, Changchun Institute of Applied Chemistry, CAS, Changchun 130022, China. E-mail: hdwang@ciac.jl.cn*

[c]*Institute of Polymer Optoelectronic Materials & Devices, State Key Laboratory of Luminescent Materials & Devices, South China University of Technology, Guangzhou, 510640, China. E-mail: msfhuang@scut.edu.cn*

[d]*Hebei Key Laboratory of Applied Chemistry, School of Environmental and Chemical Engineering, Yanshan University, Qinghuangdao 066004, China*

† Electronic supplementary information (ESI) available. See DOI: 10.1039/c3nr02522e

‡ H. Liu, X. Hao, C. H. Duan, and H. Yang contributed equally to this work.

examples of fluorescent sensors based on small molecules have been reported for Al^{3+} detection.[10–15] Moreover, most of the reported Al^{3+} sensors suffer from the disadvantages of complicated synthetic procedures and/or lack of practical applicability in aqueous media.[4,10,11,13–19] Therefore, it remains highly desirable to develop new probes for the selective evaluation of Al^{3+} in aqueous media for environmental and biological studies. NPs consisting primarily of conjugated polymers have emerged as a novel type of fluorescent probe for fluorescence detection owing to their salient features which include relatively high brightness, large absorption cross sections, and good photostability.[20–23] Recently, Chiu and co-workers reported the use of conjugated polymer nanoparticles (CPNs) as fluorescent probes for the detection of Cu^{2+} and Fe^{2+}, based on the sensing mechanism of aggregation-induced fluorescence quenching.[24] Moreover, CPN probes were developed very recently for Hg^{2+} sensing in Harbron's group[25] and for Cu^{2+} sensing in Chan's group,[26] both based on the Förster (fluorescence) resonance energy transfer (FRET) mechanism. However, the exploitation of CPN-based fluorescent probes for the detection of Al^{3+} remains unexplored and no example of such probes for Al^{3+} sensing in live cells has been reported thus far.

In this article, we report the construction, spectroscopic properties, and the preliminary intracellular fluorescence imaging results of a new type of far-red fluorescent probe for selective Al^{3+} sensing in aqueous media. Of particular note is that this type of probe displays Al^{3+}-induced far-red fluorescence (centered ~710 nm) enhancement, significantly different from the above mentioned metal ion mediated fluorescence quenching of CPN probes.[24] In terms of detection sensitivity and selectivity, the measurement of high or analyte-enhanced emission signals is analytically favored as compared to an analyte-induced quenching/decrease of a specific fluorescence.[27] Additionally, fluorescence emission with wavelengths in the biological window of maximum optical transparency (~700 to 1000 nm) is expected to impart a salient advantage for biological detection applications to these as-prepared probes. It is also worth mentioning that this type of Al^{3+} probe is easily suspended in aqueous solutions, indicating their practical applicability in physiological media. To the best of our knowledge, this is the first paradigm where a CPN-based probe functions in aqueous media and displays Al^{3+}-induced far-red fluorescence enhancement. Such feature-packed probes are expected to further advance Al^{3+} sensing capabilities in practical biological systems.

2 Results and discussion

The CPN-based Al^{3+} probes in the present work were constructed from a type of far-red fluorescent conjugated polymer, PCzDCN, and a polystyrene-based amphiphilic polymer, PST–SO_3H, *via* a reprecipitation strategy.[24–26,28] As shown in Fig. 1, PCzDCN possesses a carbazole-based two-dimensional donor–π bridge–acceptor (D–π–A) structure with the electron acceptors located at the end of the polymer side chains, which entails strong intramolecular charge transfer (ICT) interactions between its conjugated backbone and the pendant acceptor

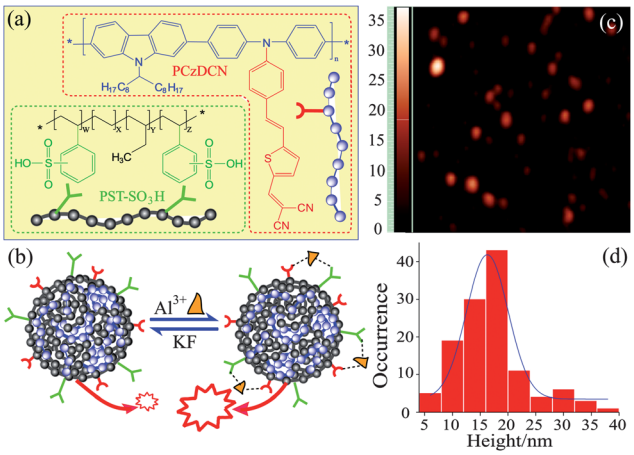

Fig. 1 (a) Chemical structures of the far-red fluorescent conjugated polymer (PCzDCN) and amphiphilic polymer, sulfonated polystyrene-*block*-poly(ethylene-ran-butylene)-*block*-polystyrene (PST–SO_3H), (b) illustration showing Al^{3+}-induced fluorescence enhancement of the PCzDCN/PST–SO_3H NPs, (c) typical AFM image (2 × 2 μm) of the as-prepared PCzDCN/PST–SO_3H polymer NPs and histogram of the particle height (d).

groups.[29] PCzDCN was initially designed and synthesized for use in polymer bulk heterojunction (BHJ) solar cells as an electron-donor material owing to its good charge transport properties.[29] On the other hand, PCzDCN is intrinsically endowed with potential for ICT-based metal ion sensing due to its unique structure with a strong electron acceptor and a strong electron-releasing receptor within a two-dimensional D–π–A skeleton.[27] PST–SO_3H polymers consist of hydrophobic alkyl main chains and side chains bearing hydrophilic sulfonated styrene units (ST–SO_3H). During the reprecipitation, the hydrophobic alkyl main chains of PST–SO_3H are prone to entwine with PCzDCN's main chains due to hydrophobic interactions in aqueous media, and therefore form a hydrophobic core, while the hydrophilic side chains of PST–SO_3H reside on the surface of the polymer NPs, providing coordination sites for metal ions.[24] The Fourier transform infrared spectroscopy (FTIR) characterization of the as-prepared complex NPs confirmed the involvement of both PCzDCN and PST–SO_3H components in the NPs (Fig. S1†). The shape of the as-prepared complex NPs was characterized by Atomic Force Microscopy (AFM), which shows a spherical shape with an average diameter of ~18 nm. The AFM characterization results are roughly in accordance with the Transmission Electron Microscopy (TEM) measurements (Fig. S2†). Dynamic light scattering (DLS) measurement of the same NPs sample reports an average hydrodynamic diameter of ~23 nm and a relatively narrow polydispersity of less than 10%. Though these measurements were for the same NPs sample as the AFM and TEM measurements, the fact that the DLS measurement was carried out with the NPs suspended in an aqueous environment while the AFM and TEM measurements were performed with dry NPs is the most likely reason for the observed discrepancy in diameter results, *i.e.* hydrodynamic swelling would have led to a larger measured diameter in the case of DLS.[30] The zeta potential of the aqueous dispersion containing the as-prepared

NPs is approximately −46 mV, indicating good stability of the as-prepared NPs sample.

The as-prepared PCzDCN/PST–SO_3H NPs probes display Al^{3+}-sensitive fluorescence emission features, as shown in Fig. 2. Upon excitation at 543 nm, the PCzDCN/PST–SO_3H NPs aqueous dispersion emits far-red fluorescence centered at 710 nm. The addition of small aliquots of Al^{3+} to the dispersion sample clearly induces an increase in the emission intensity at 710 nm and such fluorescence enhancement is gradually augmented upon further incremental addition of Al^{3+} up to 85 μM. No further enhancement in fluorescence intensity was observed upon increasing the Al^{3+} concentration above 85 μM, indicating a saturated state of the PCzDCN/PST–SO_3H NPs with respect to Al^{3+}. A plot of $(I - I_0)/I_0$ against the concentration of Al^{3+} ranging from 0 to 85 μM, and the corresponding linear fit ($R^2 = 0.996$) is presented in Fig. 2b. From titrations, a detection limit of 35 ppb of the as-prepared PCzDCN/PST–SO_3H NPs probe for Al^{3+} was obtained. The detection limit of 35 ppb of the as-prepared probes definitely imparts the ability to reliably sense the Al^{3+} concentration in drinking water with respect to the U. S. EPA limit and the EU standard (~200 ppb). Based on clinical symptomatologies associated with aluminium, 50 ppb aluminium is generally considered to be a reasonable "limit" below which aluminium neurotoxicity is not likely to occur.[31] Moreover, a serum aluminium content of greater than 50 ppb is consistent with overload and may correlate with toxicity, according to the interpretive data that the U.S. ARUP National Reference Laboratory established. Thus, the Al^{3+} probe developed in this work is more than sufficient for the detection of Al^{3+} concentration in serum or plasma samples for practical applications.

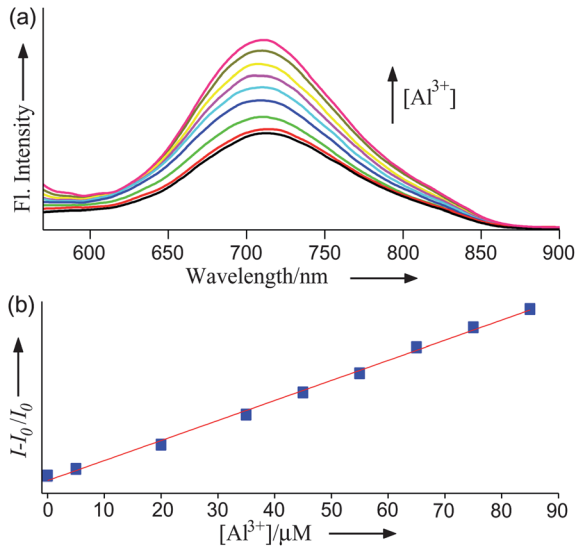

Fig. 2 (a) Fluorescence spectra evolution of PCzDCN/PST–SO_3H NPs aqueous dispersion upon changing the Al^{3+} concentration, excited at 543 nm. (b) A plot of the ratio of $I : I_0$ over I_0 as a function of Al^{3+} concentration. I_0 is the integrated emission intensities of the polymer NPs aqueous dispersion in the absence of Al^{3+} and I is the counterpart intensity in the presence of different concentrations of Al^{3+}. The red line is a linear fit to the data ($R^2 = 0.996$).

To evaluate the ion selectivity of this type of Al^{3+} probe, the PCzDCN/PST–SO_3H NPs were tested against various other physiologically important metal ions such as Li^+, Na^+, K^+, Ag^+, Cu^{2+}, Fe^{2+}, Mg^{2+}, Mn^{2+}, Zn^{2+}, Ni^{2+}, Co^{2+}, Ca^{2+}, Pb^{2+}, and Fe^{3+}. As shown in Fig. 3, upon addition of these reference metal ions with identical concentrations, the fluorescence emission intensity of the PCzDCN/PST–SO_3H NPs aqueous sample was either unchanged or minimally affected compared to the emission intensity of PCzDCN/PST–SO_3H NPs in the absence of metal ions. Specifically, the fluorescence intensity of the NPs probes remained almost unchanged upon the introduction of Mg^{2+}, Mn^{2+}, and Zn^{2+}. A slight decrease in the fluorescence intensity of the NPs probes was induced by the presence of Cu^{2+}, Li^+, Na^+, Co^{2+}, Ag^+, Fe^{2+}, K^+ and Ni^{2+}, showing a striking contrast with the Al^{3+}-induced fluorescence enhancement. Additionally, Ca^{2+}, Pb^{2+}, and Fe^{3+} were found to lead to a slight enhancement of emission intensity, with a maximum enhancement of 8.6% in the case of Fe^{3+}. In sharp contrast to the effect that these reference cations exert on the fluorescence emission intensity of the NPs probes, the presence of Al^{3+} induced a fluorescence enhancement of up to 213%, indicating a high selectivity of the as-prepared PCzDCN/PST–SO_3H NPs probes for Al^{3+}.

For fluorescent sensors which display increased or turn-on fluorescence in response to ions or signalling molecules, the photophysical and photochemical mechanisms involved are rather diverse and in many cases remain largely obscure.[27] DLS measurements of a PCzDCN/PST–SO_3H NPs aqueous suspension sample after the addition of Al^{3+} revealed an apparent increase in the average hydrodynamic diameter of about ~240 nm, as compared to the sample prior to the addition of Al^{3+}, as shown in Fig. 4a and b. Additionally, obvious scattering features in the short-wavelength region in the UV-Vis spectra of the NPs aqueous suspension sample were observed after the addition of Al^{3+} (Fig. 4c), confirming the formation of larger aggregates of NPs. It is also noteworthy that in the present work, the PCzDCN/PST–SO_3H NPs showed fluorescence enhancement upon addition of Al^{3+} and subsequently displayed fluorescence reversion upon further introduction of KF, which functions as an Al^{3+} chelator for the sequestration of Al^{3+} (Fig. 4d). Such

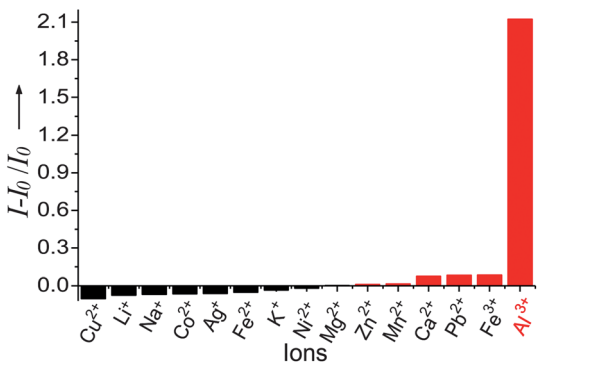

Fig. 3 Effects of different cations on the far-red fluorescence intensity (at 710 nm) of the PCzDCN/PST–SO_3H polymer NPs. The red bars represent an increase in the ion-induced fluorescence intensity while the gray bars represent a decrease in the ion-induced fluorescence intensity.

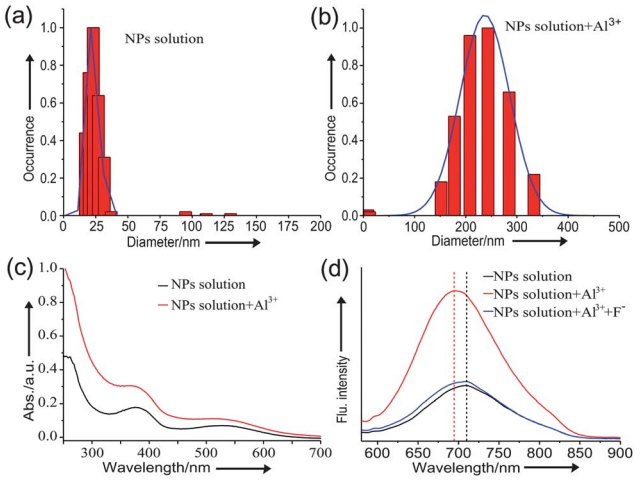

Fig. 4 (a) and (b) Dynamic light scattering measurements of the PCzDCN/PST–SO_3H NPs prior to and after addition of Al^{3+}; (c) effect of Al^{3+} on the absorption features of a PCzDCN/PST–SO_3H NPs aqueous dispersion sample; (d) effect of Al^{3+} on the fluorescence emission features of the PCzDCN/PST–SO_3H NPs aqueous dispersion sample.

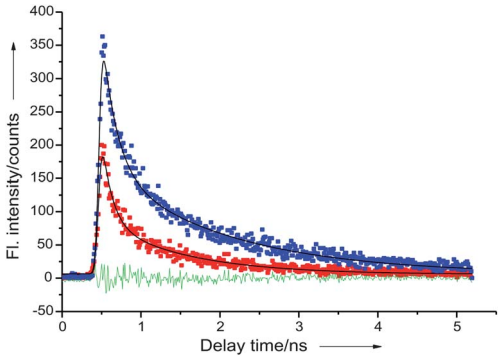

Fig. 5 (A) Picosecond time-resolved fluorescence kinetics (at 710 nm) of PCzDCN/PST–SO_3H NPs aqueous dispersions in the absence of Al^{3+} (red solid squares) and in the presence of Al^{3+} (blue solid squares). The scattered symbols represent experimental data and the black solid lines are fits. The green curve is the residual. The temporal resolution was ~35 ps.

reversibility of the fluorescence emission indicates that the Al^{3+}-induced fluorescence enhancement did not arise from a reaction-based activation mechanism, in which an irreversible reaction between usually weakly fluorescent probes with metal ions leads to the formation of a relatively highly fluorescent product.[32] As mentioned above, the addition of Al^{3+} induced the formation of aggregates of NPs with relative large diameters, which is usually accompanied by fluorescence self-quenching phenomena as reported by Chiu *et al.*[24] Taking into account the observed Al^{3+}-induced increase, as opposed to decrease, in the fluorescence emission of the PCzDCN/PST–SO_3H NPs in the present work, it is reasonable to infer that another "positive" effect was involved which more than offset the aggregation-induced fluorescence self-quenching.

Taking into account the two-dimensional D–π–A structure of the PCzDCN component, it is proposed that an Al^{3+}-dependent ICT process is the main contributor to the observed response in fluorescence emission to Al^{3+}. Such speculation was supported by the picosecond time-resolved fluorescence spectroscopy measurement results of PCzDCN/PST–SO_3H NPs aqueous suspension in both the absence and presence of Al^{3+}, which is expected to provide information regarding the excited state behaviour of the fluorescent probe. The fluorescence decay curves were fitted with a bi-exponential function with acceptable χ^2, as shown in Fig. 5. In the absence of Al^{3+}, the PCzDCN/PST–SO_3H NPs aqueous suspension displayed an average fluorescence lifetime of 437 ps, which is consistent with the lifetime results of CPNs constructed from conjugated polymers with similar chemical structures.[33] Upon addition of Al^{3+}, the number of detected photons clearly increased and simultaneously the average fluorescence lifetime of the PCzDCN/PST–SO_3H NPs aqueous suspension sample was found to increase up to 737 ps, suggesting a change in the excited state of the PCzDCN fluorescent component in the particles. Specifically, such a prolonged fluorescence lifetime is attributable to an Al^{3+}-triggered inhibition of the ICT processes from the donor groups on the polymer backbone chain to the acceptors at the end of the side chains[34] and the radiationless deactivation channels of the excited PCzDCN component.[35] Such inhibition of the radiationless deactivation channels is expected to enable more excited-state species to relax to the ground state *via* photon emission and therefore contributes to the enhanced fluorescence emission intensity. Another noteworthy feature of the fluorescence emission of PCzDCN/PST–SO_3H NPs is a 15 nm hypsochromic shift from 710 nm to 695 nm upon addition of Al^{3+}, as shown in Fig. 4d. Together with the above-mentioned chelation-induced fluorescence enhancement and increase in the average fluorescence lifetime, such a hypsochromic shift in the fluorescence emission spectra provides a coherent picture of the Al^{3+}-triggered inhibition of the ICT process.[36]

Another piece of information derived from the Al^{3+}-induced change in the fluorescence lifetime of PCzDCN/PS–SO_3H NPs is the direct involvement of the PCzDCN component in Al^{3+} chelating/binding. On the other hand, the indispensable role of the amphiphilic polymer PST-SO_3H in the Al^{3+} sensing ability of the complex PCzDCN/PST–SO_3H NPs was also experimentally confirmed, and the ratio of sulfonated styrene units (ST–SO_3H) to the fluorescent polymer in the complex NPs was found to exert significant influence on the Al^{3+}-induced fluorescence enhancement (Fig. S3†). Specifically, it was found that PCzDCN NPs fabricated without the PST–SO_3H component clearly showed Al^{3+}-independent fluorescence emission features. As shown in Fig. 6, the fluorescence emission spectrum of the PCzDCN NPs aqueous dispersion sample in the presence of Al^{3+} is nearly identical to that of the sample in the absence of Al^{3+}, clearly suggesting the indispensable chelating role of the PST–SO_3H component. In light of this, we believe that both the PCzDCN and PST–SO_3H components participate in the Al^{3+}-chelating/binding processes, while the former simultaneously acts as the ion recognition and signalling site. Specifically, the involvement of PCzDCN components in cooperative chelation processes intrinsically enables an Al^{3+}-triggered inhibition effect on the ICT processes. Thus the observed Al^{3+}-induced fluorescence enhancement of the as-prepared PCzDCN/PST–SO_3H NPs is actually a result of two opposing effects,

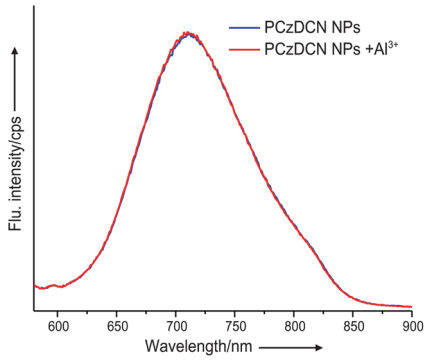

Fig. 6 Effect of Al^{3+} on the fluorescence emission features of a PCzDCN NPs aqueous dispersion sample.

namely aggregation-induced fluorescence self-quenching and Al^{3+}-triggered ICT inhibition, with the latter playing a predominant role and more than offsetting the former. Such speculation is supported by the steady-state and transient fluorescence spectroscopy characterization results, as discussed above.

To test the practicability of Al^{3+} ion sensing by the as-prepared PCzDCN/PST–SO_3H NPs in intracellular milieu, Vero cells internalized with PCzDCN/PST–SO_3H NPs probes (*ca.* 1 μM) were treated with $AlCl_3$-containing Dulbecco's Modified Eagle medium (DMEM) and time-lapsed *in situ* fluorescence images were collected using a Nikon eclipse Ti inverted microscope. For intracellular applications of functional probes, it is desirable to be able to escort the probes directly into the cell in a way that is facile, noninvasive, and nonstressful for the cells.[37] As compared to those membrane-permeable organic dyes and probes functionalized with cell-penetrating peptides, the use of NPs for intracellular imaging is generally complicated by the challenge of escorting the nanoparticle-based probes to the interior of the cells. For the cell experiments in the present work, it was found that the PCzDCN/PST–SO_3H NPs with surface-bound negatively charged sulfonic acid groups could cross the cell membranes with ease and enter cells without the assistance of any delivery vectors. It is proposed that this type of nanoparticle crossed the cell membrane and entered into cells *via* a self-loading mechanism, similar to that reported previously by our group for polymer NPs with surface-bound negatively charged carboxyl groups.[38] This feature of easy ingestion of the as-prepared probes is in sharp contrast to those facilitated by endocytosis processes, although additional investigation is required to gain a better understanding of the detailed underlying mechanism and factors affecting nanoparticle uptake as well as the fate of the internalized particles. In a typical protocol for cell ingestion, Vero cells were incubated with PCzDCN/PST–SO_3H NPs probes at 37 °C for 1 h and then washed with warm PBS buffer three times prior to the subsequent intracellular Al^{3+} sensing experiments. The fluorescence images of these pre-treated Vero cells indicated the internalization of the PCzDCN/PST–SO_3H NPs by the cells and most internalized NPs were transported to late endosomes and lysosomes, which is consistent with other types of polymer NPs with surface-bound negatively charged groups for intracellular imaging.[39]

It is worth mentioning that the mechanism of aluminium absorption is not well understood, but appears to involve active transport as well as passive diffusion. Transferrin, the major iron transport protein in plasma, is generally believed to act as the carrier for the active transport mechanism, while a concentration gradient is required to initiate the passive diffusion from the medium into the cells.[40,41] To stimulate the uptake of Al^{3+} ions into cells, aliquots of DMEM medium with Al^{3+} concentrations ranging from tens to hundreds of μM were used to replace the original DMEM medium and then time-lapsed *in situ* fluorescence images of the Vero cells with internalized PCzDCN/PST–SO_3H NPs were acquired. Fig. 7a displays three typical images acquired at different stages after replacement of the Al^{3+}-free medium with Al^{3+}-containing medium, and shows a distinct discrepancy in the fluorescence brightness. Specifically, distinctly enhanced fluorescence was observed soon after the replacement of medium, indicating the occurrence of Al^{3+} ion influx and the intracellular Al^{3+}-chelating/binding of PCzDCN/PST–SO_3H NPs (Fig. S4†). Additionally, the fluorescence intensity peaked after approximately 8 min with a 10.8 times fluorescence enhancement. After the peak value, the fluorescence intensity gradually decreased with time and finally stabilized after 30 min with an intensity 6 times stronger than that before addition of $AlCl_3$, as shown in Fig. 7b. As a control experiment, fluorescence images of Vero cells internalized with PCzDCN/PST–SO_3H NPs probes were acquired under identical conditions except in DMEM without the addition of $AlCl_3$. It can clearly be seen from Fig. 8 that no detectable fluorescence enhancement was observed. In reverse, a continuous decrease in fluorescence intensity was observed, possibly as a result of photobleaching arising from the continuous laser illumination (Fig. S5†). Such sharp contrast in the fluorescence emission features of the as-prepared PCzDCN/PST–SO_3H NPs probes in both the absence and presence Al^{3+} confirms the vital role of Al^{3+} in inducing the fluorescence enhancement in intracellular milieu, and also verifies the Al^{3+}-sensing ability of the PCzDCN/PST–SO_3H NPs.

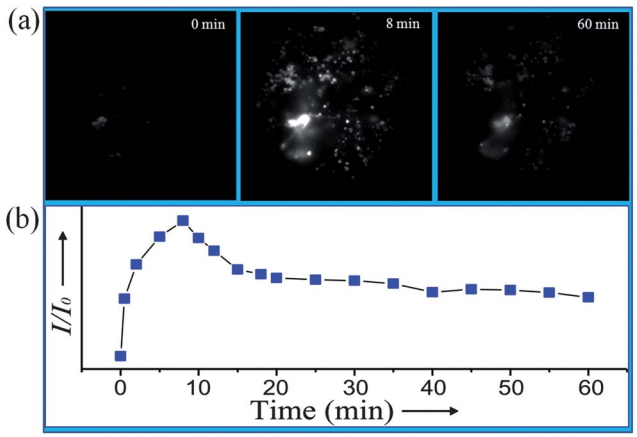

Fig. 7 (a) Time-lapse fluorescence images of Vero cells with internalized PCzDCN/PST–SO_3H NPs in Dulbecco's Modified Eagle medium (DMEM) containing 170 μM Al^{3+}. (b) A plot of I/I_0 as a function of cell incubation time in $AlCl_3$-containing DMEM. For each time point, the fluorescence intensity inside the target cell was acquired with the use of the ImageJ image processing program, public domain software developed at the National Institutes of Health.

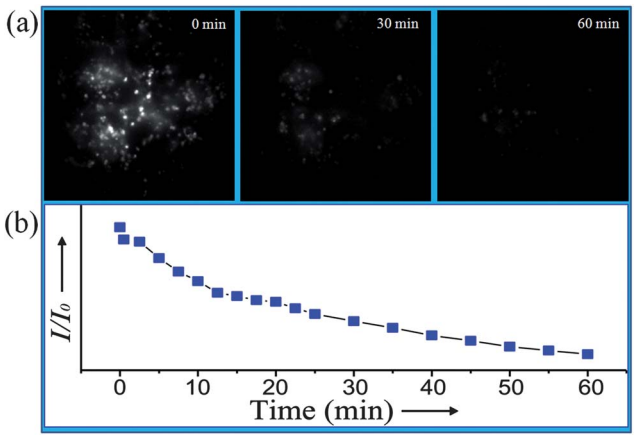

Fig. 8 Time-lapse intracellular fluorescence imaging of Vero cells with internalized PCzDCN/PST–SO_3H NPs in Al^{3+}-free Dulbecco's Modified Eagle medium DMEM buffer.

Why the as-prepared PCzDCN/PST–SO_3H NPs showed stronger Al^{3+}-induced fluorescence enhancement in intracellular milieu as compared to that in extracellular milieu remains a mystery, though the enrichment of the Al^{3+} ions and PCzDCN/PST–SO_3H NPs probes in specific organelles is the most likely explanation for the observed discrepancy. The intracellular metabolism of aluminium is poorly understood but presumably it follows the pathways of iron metabolism, being incorporated with transferrin-bound iron into endosomes. In certain human pathologies as well as in experimental animals, aluminium has been observed to accumulate preferentially inside lysosomes, which raises the possibility that lysosomes serve as an elective site of aluminium accumulation.[42–44] On the other hand, as previously mentioned, most PCzDCN/PST–SO_3H NPs internalized by the Vero cells were transported to lysosomes. Thus the lysosomes actually act as a location for enrichment of both Al^{3+} and the Al^{3+} probes. As a result, with Al^{3+} chelating/binding *via* the PCzDCN components, a strengthening of ICT inhibition is expected and a more remarkable fluorescence enhancement was consequently observed. Further investigation on the detailed mechanism is underway.

3 Conclusions

In conclusion, we have described the synthesis, properties, and preliminary intracellular application of a new far-red fluorescent probe for Al^{3+} sensing and imaging. As a result of inclusion of the two-dimensional D–π–A structure with strong electron acceptors located at the end of the polymer side chains, this new probe displayed distinctly enhanced far-red fluorescence emission (~710 nm) in selective response to the presence of the Al^{3+} ion. It is believed that the observed Al^{3+}-induced fluorescence enhancement in the present work originates from two opposing effects, namely, aggregation-induced fluorescence self-quenching and Al^{3+}-triggered inhibition on the ICT process between the conjugated backbone and the pendant acceptors, with the latter playing a predominant role and more than offsetting the former. This proposed mechanism was supported by the steady-state and transient fluorescence spectroscopy characterization results. The as-prepared Al^{3+} displayed a detection limit of 35 ppb, which is more than sufficient for the sensing of Al^{3+} concentrations in drinking water, serum or plasma samples. Moreover, preliminary fluorescence imaging experiments have revealed the facile cellular ingestion and biocompatibility of the as-prepared probes, and validated their practicability for Al^{3+} ion mapping in living cells. We are actively pursuing probes with optimized performance for the fluorescence imaging of Al^{3+} ions in living cells, and the application of these probes for investigations on Al^{3+}-related physiological and pathological processes.

4 Experimental details

The conjugated polymer PCzDCN (average M_w 12 500, polydispersity 1.7) was synthesized according to the literature.[29] The amphiphilic polymer PST–SO_3H (styrene, 29 wt%, sulfonated styrene units, 55–65%, Sigma-Aldrich) was purchased as 5 wt% in 1-propanol and dichloromethane, and the solvents were replaced with tetrahydrofuran (THF) for the final construction of the PCzDCN/PST–SO_3H NPs *via* a reprecipitation strategy.

Preparation of PCzDCN/PST–SO_3H NPs: a homogeneous solution (500 μL) of PCzDCN and PST–SO_3H in THF was rapidly injected into 8 mL of deionized water under brief sonication. The THF was removed by partial vacuum evaporation and the resulting nanoparticle suspension was filtered through a 0.22 micron membrane filter (Millipore) to remove larger aggregates, giving clear bright nanoparticle dispersions which were stable for weeks without noticeable signs of aggregation.

For the determination of nanoparticle diameter by AFM, a clean coverslip was silanized with 3-aminopropyl-trimethoxysilane and then one drop of the nanoparticle dispersion was placed on the silanized glass surface. After evaporation of the water, the surface topography (5 × 5 μm) was imaged with an NTEGRA/SOLVER system (NT-MDT Co.) using tapping mode in air. Dynamic light scattering (DLS) measurements were carried out on a Nicomp 380 ZLS Particle Size Analyzer at a scattering angle of 90°, with the 632.8 line of a He–Ne laser as an excitation source. The FT-IR spectrum of the as-prepared PCzDCN/PST–SO_3H NPs was acquired from a thin layer of aqueous NPs dispersion sample between two silicon wafers using a Bruker Vertex 80 spectrometer. The NPs sample for TEM characterization was prepared by placing a drop of the as-prepared PCzDCN/PS–SO_3H NPs aqueous dispersion on a carbon-coated Cu grid, followed by solvent evaporation at room temperature. The TEM characterization was performed using a Tecnai G^2 20 S-TWIN.

Fluorescence lifetimes were determined using a picoseconds time-resolved fluorescence apparatus that has been described elsewhere.[45] Briefly, the 460 nm excitation laser pulses were supplied by an optical parametric amplifier (OPA-800CF, Spectra Physics), which was pumped by a regenerative amplifier (Spitfire, Spectra Physics). The excitation pulse energy was ~100 nJ per pulse with a pulse repetition rate of 1 kHz and it was focused onto a spot of 0.5 mm in diameter. Photoluminescence collected with a 90° geometry was dispersed by a

polychromator (250is, Chromex) and collected with a photon-counting type streak camera (C5680, Hamamatsu Photonics). The data detected by the digital camera (C4742-95, Hamamatsu) were routinely transferred to a PC for analysis with HPDTA software. The spectral resolution was 2 nm and the temporal resolution was 2–100 ps depending on the delay-time range setting. Analysis of the kinetic traces derived from time-resolved spectra was performed individually using nonlinear least-square fitting to a general sum-of-exponentials function after deconvolution of the instrument response function (IRF). All of the spectroscopic measurements were carried out at room temperature.

Cell culture and co-incubation with PCzDCN/PST–SO_3H NPs probes: Vero cell lines were maintained in a 5% CO_2 environment at 37 °C in Dulbecco's Modified Eagle medium (DMEM) supplemented with 10% (vol/vol) FBS (HyClone), 100 international units per mL penicillin, and 100 μg per mL streptomycin. For fluorescence imaging, Vero cells were cultured for 24–48 hours to achieve 75% confluence in the same medium in 35 mm glass-bottom culture dishes. Before experiments, cells were washed with DMEM (phenol red-free) and then kept in this medium for experiments. The probe dispersions (20 μL, *ca.* 1 μM) were added to cell media (200 μL) and allowed to incubate for 1–2 h. The cells were then washed 3 times with warm PBS buffer (NaCl 137 mM, KCl 2.7 mM, Na_2HPO_4 10 mM, KH_2PO_4 2 mM, pH 7.4).

For cell fluorescence imaging, Vero cells were internalized with Al^{3+} probes at 37 °C for 1–2 hours and the fluorescence images of the Al^{3+} probes in living cells were captured. Subsequently, the original cell culture medium was replaced with DMEM containing $AlCl_3$ and the *in situ* sequential fluorescence images were immediately collected using a Nikon eclipse Ti inverted microscope equipped with a 532 nm solid laser and a 100× oil-immersion objective (1.49 NA). The laser beam was coupled by dichroic mirrors and widened by a telescope consisting of achromatic doublet lenses before injection into the microscope with typical laser intensities of approximately 200 μW in the center of the laser spot in the sample plane. The emission lights were filtered with a long-pass filter (600 nm) and imaged on an EMCCD camera (Photometrics, Cascade II). The image plane used for recording in all experiments was approximately 2 μm thick. All fluorescence image exposure times were 100 ms unless otherwise stated. For the control experiment, sequential fluorescence images of cells internalized with Al^{3+} probes in DMEM in the absence of $AlCl_3$ were acquired following the identical procedure. The intensities of the fluorescence images were analysed by ImageJ.

Acknowledgements

The authors thank Dr Y. S. Wu and Prof. H. B. Fu at Institute of Chemistry, CAS for their assistance in the picosecond time-resolved fluorescence kinetics measurements. Financial support from the National Natural Science Foundation of China (grant no. 21173262, 21073181, 21125419), MOST (grant no. 2011CB933600, 2009CB623601), and the "Hundred-Talent Program" of CAS to ZT and HW are acknowledged.

References

1 G. H. Robinson, *Chem. Eng. News*, 2003, **81**, 54.
2 T. L. Macdonald and R. B. Martin, *Trends Biochem. Sci.*, 1988, **13**, 15–19.
3 *Metal Ions in Biological Systems*, ed. A. Sigel and H. Sigel, 1988, vol. 24.
4 D. Maity and T. Govindaraju, *Inorg. Chem.*, 2010, **49**, 7229–7231.
5 P. Nayak, *Environ. Res.*, 2002, **89**, 101–115.
6 G. Lupidi, M. Angeletti, A. M. Eleuteri, E. Fioretti, S. Marini, M. Gioia and M. Coletta, *Coord. Chem. Rev.*, 2002, **228**, 263–269.
7 D. P. Perl and A. R. Brody, *Science*, 1980, **208**, 297–299.
8 D. P. Perl, D. C. Gajdusek, R. M. Garruto, R. T. Yanagihara and C. J. Gibbs, *Science*, 1982, **217**, 1053–1055.
9 K. Soroka, R. S. Vithanage, D. A. Phillips, B. Walker and P. K. Dasgupta, *Anal. Chem.*, 1987, **59**, 629–636.
10 X. Sun, Y. W. Wang and Y. Peng, *Org. Lett.*, 2012, **14**, 3420–3423.
11 S. Kim, J. Y. Noh, K. Y. Kim, J. H. Kim, H. K. Kang, S. W. Nam, S. H. Kim, S. Park, C. Kim and J. Kim, *Inorg. Chem.*, 2012, **51**, 3597–3602.
12 F. K. W. Hau, X. M. He, W. H. Lam and V. W. W. Yam, *Chem. Commun.*, 2011, **47**, 8778–8780.
13 Y. Lu, S. S. Huang, Y. Y. Liu, S. He, L. C. Zhao and X. S. Zeng, *Org. Lett.*, 2011, **13**, 5274–5277.
14 T. H. Ma, M. Dong, Y. M. Dong, Y. W. Wang and Y. Peng, *Chem.–Eur. J.*, 2010, **16**, 10313–10318.
15 W. Y. Lin, L. Yuan and J. B. Feng, *Eur. J. Org. Chem.*, 2008, **2008**, 3821–3825.
16 S. H. Kim, H. S. Choi, J. Kim, S. J. Lee, D. T. Quang and J. S. Kim, *Org. Lett.*, 2010, **12**, 560–563.
17 D. Maity and T. Govindaraju, *Chem. Commun.*, 2010, **46**, 4499–4501.
18 A. Ben Othman, J. W. Lee, Y. D. Huh, R. Abidi, J. S. Kim and J. Vicens, *Tetrahedron*, 2007, **63**, 10793–10800.
19 Y. W. Wang, M. X. Yu, Y. H. Yu, Z. P. Bai, Z. Shen, F. Y. Li and X. Z. You, *Tetrahedron Lett.*, 2009, **50**, 6169–6169.
20 J. Pecher and S. Mecking, *Chem. Rev.*, 2010, **110**, 6260–6279.
21 A. Kaeser and A. P. H. J. Schenning, *Adv. Mater.*, 2010, **22**, 2985–2997.
22 Z. Y. Tian, J. B. Yu, C. F. Wu, C. Szymanski and J. McNeill, *Nanoscale*, 2010, **2**, 1999–2011.
23 C. F. Wu and D. T. Chiu, *Angew. Chem., Int. Ed.*, 2013, **52**, 3086–3109.
24 Y. H. Chan, Y. H. Jin, C. F. Wu and D. T. Chiu, *Chem. Commun.*, 2011, **47**, 2820–2822.
25 E. S. Childress, C. A. Roberts, D. Y. Sherwood, C. L. M. LeGuyader and E. J. Harbron, *Anal. Chem.*, 2012, **84**, 1235–1239.
26 P. J. Wu, J. L. Chen, C. P. Chen and Y. H. Chan, *Chem. Commun.*, 2013, **49**, 898–900.
27 K. Rurack, *Spectrochim. Acta, Part A*, 2001, **57**, 2161–2195.
28 C. F. Wu, H. S. Peng, Y. F. Jiang and J. McNeill, *J. Phys. Chem. B*, 2006, **110**, 14148–14154.
29 C. H. Duan, K. S. Chen, F. Huang, H. L. Yip, S. J. Liu, J. Zhang, A. K. Y. Jen and Y. Cao, *Chem. Mater.*, 2010, **22**, 6444–6452.

30 M. Q. Zhu, L. Y. Zhu, J. J. Han, W. W. Wu, J. K. Hurst and A. D. Q. Li, *J. Am. Chem. Soc.*, 2006, **128**, 4303–4309.
31 T. P. Flaten, A. C. Alfrey, J. D. Birchall, J. Savory and R. A. Yokel, Status and Future Concerns of Clinical and Environmental Aluminum Toxicity, in *Research Issues in Aluminum Toxicity*, ed. R. A. Yokel and M. S. Golub, CRC Press, Vancouver, 1997, pp. 1–11.
32 A. R. Lippert, E. J. New and C. J. Chang, *J. Am. Chem. Soc.*, 2011, **133**, 10078–10080.
33 C. F. Wu, B. Bull, C. Szymanski, K. Christensen and J. McNeill, *ACS Nano*, 2008, **2**, 2415–2423.
34 X. F. Zhou, F. Y. Su, Y. Q. Tian, C. Youngbull, R. H. Johnson and D. R. Meldrum, *J. Am. Chem. Soc.*, 2011, **133**, 18530–18533.
35 S. Jana, S. Dalapati, M. A. Alam and N. Guchhaita, *J. Photochem. Photobiol., A*, 2012, **238**, 7–15.
36 S. Das, D. Karak, S. Lohar, A. Banerjee, A. Sahana and D. Das, *Anal. Methods*, 2012, **4**, 3620–3624.
37 R. I. Dmitriev and D. B. Papkovsky, *Cell. Mol. Life Sci.*, 2012, **69**, 2025–2039.
38 H. Liu, H. Yang, X. Hao, H. J. Xu, Y. Lv, D. B. Xiao, H. D. Wang and Z. Y. Tian, *Small*, 2013, **9**, 2639–2648.
39 Z. Y. Tian, W. W. Wu, W. Wan and A. D. Q. Li, *J. Am. Chem. Soc.*, 2009, **131**, 4245–4252.
40 R. B. Martin, Aluminium speciation in biology, in *Aluminum in Biology and Medicine*, ed. D. J. Chadwick and J. Whela, Wiley, New York, 1992, pp. 5–25.
41 W. R. Harris, G. Berthon, J. P. Day, C. Exley, T. P. Flaten, W. F. Forbes, T. Kiss, C. Orvig and P. F. Zatta, Speciation of aluminum in biological systems, in *Research Issues in Aluminum Toxicity*, ed. R. A. Yokel and M. S. Golub, Taylor & Francis, New York, 1997, pp. 91–116.
42 P. Galle, M. Chatel, J. P. Berry and F. Menault, *Nouv. Presse Med.*, 1979, **8**, 4091–4094.
43 A. Roth, C. Nogues, P. Galle and T. Drueke, *Virchows Arch.*, 1984, **405**, 131–140.
44 P. Zatta, A. Taylor, P. Zambenedetti, R. Milacic and P. Antone, *Life Sci.*, 2000, **66**, 2261–2266.
45 Y. S. Wu, J. Li, X. C. Ai, L. M. Fu, J. P. Zhang, Y. Q. Fu, J. J. Zhou, L. Li and Z. S. Bo, *J. Phys. Chem. A*, 2007, **111**, 11473–11479.